



STAMPATO NEL MESE DI OTTOBRE 2007  
PRESSO IL DIPARTIMENTO DI MATEMATICA E APPLICAZIONI,  
UNIVERSITÀ DEGLI STUDI DI MILANO-BICOCCA, VIA R. COZZI 53, 20125 MILANO, ITALIA.

DISPONIBILE IN FORMATO ELETTRONICO SUL SITO [www.matapp.unimib.it](http://www.matapp.unimib.it).  
SEGRETERIA DI REDAZIONE: Ada Osmetti - Giuseppina Cogliandro  
tel.: +39 02 6448 5755-5758 fax: +39 02 6448 5705

**Esemplare fuori commercio per il deposito legale agli effetti della Legge 15 aprile 2004  
n.106.**

# TRUNCATED DECOMPOSITIONS AND FILTERING METHODS WITH REFLECTIVE/ANTI-REFLECTIVE BOUNDARY CONDITIONS: A COMPARISON

C. TABLINO POSSIO\*

**Abstract.** The paper analyzes and compares some spectral filtering methods as truncated singular/eigen-value decompositions and Tikhonov/Re-blurring regularizations in the case of the recently proposed Reflective [18] and Anti-Reflective [21] boundary conditions. We give numerical evidence to the fact that spectral decompositions (SDs) provide a good image restoration quality and this is true in particular for the Anti-Reflective SD, despite the loss of orthogonality in the associated transform. The related computational cost is comparable with previously known spectral decompositions, and results substantially lower than the singular value decomposition. The model extension to the cross-channel blurring phenomenon of color images is also considered and the related spectral filtering methods are suitably adapted.

**Key words.** filtering methods, spectral decompositions, boundary conditions.

**AMS subject classifications.** 65F10, 65F15, 65Y20

**1. INTRODUCTION.** In this paper we deal with the classical image restoration problem of blurred and noisy images in the case of a space invariant blurring. Under such assumption the image formation process is modelled according to the following integral equation with space invariant kernel

$$g(x) = \int h(x - \tilde{x})f(\tilde{x})d\tilde{x} + \eta(x), \quad x \in \mathbb{R}^2, \quad (1.1)$$

where  $f$  denotes the true physical object to be restored,  $g$  is the recorded blurred and noisy image,  $\eta$  takes into account unknown errors in the collected data, e.g. measurement errors and noise.

As customary, we consider the discretization of (1.1) by means of a standard 2D generalization of the rectangle quadrature formula on an equispaced grid, ordered row-wise from the top-left corner to the bottom-right one. Hence, we obtain the relations

$$g_i = \sum_{j \in \mathbb{Z}^2} h_{i-j} f_j + \eta_i, \quad i \in \mathbb{Z}^2, \quad (1.2)$$

in which an infinite and a shift-invariant matrix  $\tilde{A}_\infty = [h_{i-j}]_{(i,j)=((i_1,i_2),(j_1,j_2))}$ , i.e., a two-level Toeplitz matrix, is involved.

In principle, (1.2) presents an infinite summation since the true image scene does not have a finite boundary. Nevertheless, the data  $g_i$  are clearly collected only at a finite number of values, so representing only a finite region of such an infinite scene. In addition, the blurring operator typically shows a finite support, so that it is completely described by a Point Spread Function (PSF) mask such as

$$h_{PSF} = [h_{i_1,i_2}]_{i_1=-q_1,\dots,q_1,i_2=-q_2,\dots,q_2} \quad (1.3)$$

---

\*Dipartimento di Matematica e Applicazioni, Università di Milano Bicocca, via Cozzi 53, 20125 Milano, Italy (crisina.tablinopossio@unimib.it). The work of the author was partially supported by MIUR 2006017542

where  $h_{i_1, i_2} \geq 0$  for any  $i_1, i_2$  and  $\sum_{i=-q}^q h_i = 1$ ,  $i = (i_1, i_2)$ ,  $q = (q_1, q_2)$  (normalization according to a suitable conservation law).

Therefore, relations (1.2) imply

$$g_i = \sum_{s=-q}^q h_s f_{i-s} + \eta_i, \quad i_1 = 1, \dots, n_1, i_2 = 1, \dots, n_2, \quad (1.4)$$

where the range of collected data defines the so called Field of View (FOV).

Once again, we are assuming that all the involved data in (1.5), similarly to (1.2), are reshaped in a row-wise ordering. In such a way we obtain the linear system

$$\tilde{A}\tilde{f} = g - \eta \quad (1.5)$$

where  $\tilde{A} \in \mathbb{R}^{N(n) \times N(n+2q)}$  is a finite principal sub-matrix of  $\tilde{A}_\infty$ , with main diagonal containing  $h_{0,0}$ ,  $\tilde{f} \in \mathbb{R}^{N(n+2q)}$ ,  $g, \eta \in \mathbb{R}^{N(n)}$  and with  $N(m) = m_1 m_2$ , for any two-index  $m = (m_1, m_2)$ .

Such a reshape is considered just to perform the theoretical analysis, since all the deblurring/denoising methods are able to deal directly with data in matrix form. For instance, it is evident that the blurring process in (1.4) consists in a discrete convolution between the PSF mask, after a rotation of  $180^\circ$ , and the proper true image data in

$$\tilde{F} = [f_{i_1, i_2}]_{i_1=-q_1+1, \dots, n_1+q_1, i_2=-q_2+1, \dots, n_2+q_2}.$$

Hereafter, with a two-index notation, we denote by  $F = [f_{i_1, i_2}]_{i_1=1, \dots, n_1, i_2=1, \dots, n_2}$  the true image inside the FOV and by  $G = [g_{i_1, i_2}]_{i_1=1, \dots, n_1, i_2=1, \dots, n_2}$  the recorded image. Thus, assuming the knowledge of PSF mask in (1.3) and of some statistical properties of  $\eta$ , the deblurring problem is defined as to restore, as best as possible, the true image  $F$  on the basis of the recorded image  $G$ . As evident from (1.4), the problem is undetermined since the number of unknowns involved in the convolution exceeds the number of recorded data. Boundary conditions (BCs) are introduced to artificially describe the scene outside the FOV: the values of unknowns outside the FOV are fixed or are defined as linear combinations of the unknowns inside the FOV, the target being to reduce (1.5) into a square linear system

$$A_n f = g - \eta \quad (1.6)$$

with  $A_n \in \mathbb{R}^{N(n) \times N(n)}$ ,  $n = (n_1, n_2)$ ,  $N(n) = n_1 n_2$  and  $f, g, \eta \in \mathbb{R}^{N(n)}$ .

The choice of the BCs does not affect the global spectral behavior of the matrix. However, it may have a valuable impact both with respect to the accuracy of the restored image and to the computational costs for recovering  $f$  from the blurred datum, with or without noise.

Notice also that, typically, the matrix  $A$  is very ill-conditioned and there is a significant intersection between the subspace related to small eigen/singular values and the high frequency subspace. Such a feature requires the use of suitable regularization methods that allow to properly restore the image  $F$  with controlled noise levels [12, 13, 14, 24], among which we can cite truncated SVD, Tikhonov, and total variation [12, 14, 24]. Hereafter, we focus our attention on special case of PSFs satisfying a strong symmetry property, i.e., such that

$$h_{|i|} = h_i \quad \text{for any } i = -q, \dots, q. \quad (1.7)$$

This assumption is fulfilled in the majority of models in real optical applications. For instance, in most 2D astronomical imaging with optical lens [5] the model of the PSF is circularly symmetric, and hence, strongly symmetric; in the multi-image deconvolution of some recent interferometric telescopes, the PSF is strongly symmetric too [6]. Moreover, in real applications when the PSF is obtained by measurements (like a guide star in astronomy), the influence of noise leads to a numerically nonsymmetric PSF, also when the kernel of the PSF is strongly (or centro) symmetric. In such a case, by employing a symmetrized version of the measured PSF, comparable restorations are observed [15, 1].

The paper is organized as follows. In Section 2 we focus on two recently proposed BCs, i.e., the Reflective [18] and Anti-Reflective BCs [21] and their relevant properties. Section 3 summarizes some classical filtering techniques as the truncated singular/eigen-values decomposition and the Tikhonov method. The Re-blurring method [11, 9] is considered in the case of Anti-Reflective BCs and its re-interpretation in the framework of the classical Tikhonov regularization is given. In Section 4 the model is generalized for taking into account the cross-channel blurring phenomenon and the previous filtering methods are suitable adapted. Lastly, Section 5 deals with some computational issues and reports several numerical tests, the aim being to compare the quoted filtering methods and the two type of BCs, both in the case of gray-scale and color images. In Section 6 some conclusions and remarks end the paper.

**2. BOUNDARY CONDITIONS.** In this section we summarize the relevant properties of two recently proposed type of BCs, i.e., the Reflective [18] and Anti-Reflective BCs [21]. Special attention is given to the structural and spectral properties of the arising matrices. In fact, though the choice of the BCs does not affect the global spectral behavior of the matrix  $A$ , it can have a valuable impact with respect both to the accuracy of the restoration (especially close to the boundaries where ringing effects can appear), and the computational costs for recovering the image from the blurred one, with or without noise.

Moreover, taking into account the scale of the problem, the regularization methods analysis can be greatly simplified whenever a spectral (or singular value) decomposition of  $A$  is easily available. This means that the target is to obtain the best possible approximation properties, keeping unaltered the fact that the arising matrix shows an exploitable structure. For instance, the use of periodic BCs enforces a circulant structure, so that the spectral decomposition can be computed efficiently with the fast Fourier transform (FFT) [8]. Despite these computational facilities, they give rise to significant ringing effects when a significant discontinuity is introduced into the image.

Hereafter, we focus on two recently proposed boundary conditions, that more carefully describe the scene outside the FOV.

Clearly, several other methods deal with this topic in the image processing literature, e.g. local mean value [22] or extrapolation techniques (see [17] and references therein). Nevertheless, the penalty of their good approximation properties could lie in a linear algebra problem more difficult to cope with.

**2.1. REFLECTIVE BOUNDARY CONDITIONS.** In [18] Ng *et al.* analyze the use of Reflective BCs, both from model and linear algebra point of view. The improvement with respect to Periodic BCs is due to the preservation of the continuity of the image. In fact, the scene outside the FOV is assumed to be a reflection of the scene inside the FOV. For example, with a boundary at  $x_1 = 0$  and  $x_2 = 0$  the

reflective condition is given by  $f(\pm x_1, \pm x_2) = f(x_1, x_2)$ .  
More precisely, along the borders, the BCs impose

$$\begin{aligned} f_{i_1, 1-i_2} &= f_{i_1, i_2}, & f_{i_1, n_2+i_2} &= f_{i_1, n_2+1-i_2}, & \text{for any } i_1 &= 1, \dots, n_1, i_2 = 1, \dots, q_2 \\ f_{1-i_1, i_2} &= f_{i_1, i_2}, & f_{n_1+i_1, i_2} &= f_{n_1+1-i_1, i_2}, & \text{for any } i_1 &= 1, \dots, q_1, i_2 = 1, \dots, n_2, \end{aligned}$$

and, at the corners, the BCs impose for any  $i_1 = 1, \dots, q_1, i_2 = 1, \dots, q_2$

$$\begin{aligned} f_{1-i_1, 1-i_2} &= f_{i_1, i_2}, & f_{n_1+i_1, n_2+i_2} &= f_{n_1+1-i_1, n_2+1-i_2}, \\ f_{1-i_1, n_2+i_2} &= f_{i_1, n_2+1-i_2}, & f_{n_1+i_1, 1-i_2} &= f_{n_1+1-i_1, i_2}, \end{aligned}$$

i.e., a double reflection, first with respect to one axis and after with respect to the other, no matter about the order.

As a consequence the rectangular matrix  $\tilde{A}$  is reduced to a square Toeplitz-plus-Hankel block matrix with Toeplitz-plus-Hankel blocks, i.e.,  $A_n$  shows the two-level Toeplitz-plus-Hankel structure. Moreover, if the blurring operator satisfies the strong symmetry condition (1.7) then the matrix  $A_n$  belongs to DCT-III matrix algebra. Therefore, its spectral decomposition can be computed very efficiently using the fast discrete cosine transform (DCT-III) [23].

More in detail, let  $\mathcal{C}_n = \{A_n \in \mathbb{R}^{N(n) \times N(n)}, n = (n_1, n_2), N(n) = n_1 n_2 \mid A_n = R_n \Lambda_n R_n^T\}$  be the two-level DCT-III matrix algebra, i.e., the algebra of matrices that are simultaneously diagonalized by the orthogonal transform

$$R_n = R_{n_1} \otimes R_{n_2}, \quad R_m = \left[ \sqrt{\frac{2 - \delta_{t,1}}{m}} \cos \left\{ \frac{(s-1)(t-1/2)\pi}{m} \right\} \right]_{s,t=1}^m, \quad (2.1)$$

with  $\delta_{s,t}$  denoting the Kronecker symbol.

Thus, the explicit structure of the matrix is  $A_n = \text{Toeplitz}(V) + \text{Hankel}(\sigma(V), J\sigma(V))$ , with  $V = [V_0 \ V_1 \ \dots \ V_{q_1} \ 0 \ \dots \ 0]$  and where each  $V_{i_1}$ ,  $i_1 = 1, \dots, q_1$  is the unilevel DCT-III matrix associated to the  $i_1^{\text{th}}$  row of the PSF mask, i.e.,  $V_{i_1} = \text{Toeplitz}(v_{i_1}) + \text{Hankel}(\sigma(v_{i_1}), J\sigma(v_{i_1}))$ , with  $v_{i_1} = [h_{i_1,0}, \dots, h_{i_1,q_2}, 0, \dots, 0]$ . Here, we denote by  $\sigma$  the shift operator such that  $\sigma(v_{i_1}) = [h_{i_1,1}, \dots, h_{i_1,q_2}, 0, \dots, 0]$  and by  $J$  the usual flip matrix; at the block level the same operations are intended in block-wise sense.

Beside this structural characterization, the spectral description is completely known. In fact, let  $f$  be the bivariate generating function associated to the PSF mask (1.3), that is

$$\begin{aligned} f(x_1, x_2) &= h_{0,0} + 2 \sum_{s_1=1}^{q_1} h_{s_1,0} \cos(s_1 x_1) + 2 \sum_{s_2=1}^{q_2} h_{0,s_2} \cos(s_2 x_2) \\ &\quad + 4 \sum_{s_1=1}^{q_1} \sum_{s_2=1}^{q_2} h_{s_1, s_2} \cos(s_1 x_1) \cos(s_2 x_2), \end{aligned} \quad (2.2)$$

then the eigenvalues of the corresponding matrix  $A_n \in \mathcal{C}_n$  are given by

$$\lambda_s(A_n) = f\left(x_{s_1}^{[n_1]}, x_{s_2}^{[n_2]}\right), \quad s = (s_1, s_2), \quad x_r^{[m]} = \frac{(r-1)\pi}{m},$$

where  $s_1 = 1, \dots, n_1, s_2 = 1, \dots, n_2$ , and where the two-index notation highlights the tensorial structure of the corresponding eigenvectors.

Lastly, notice that standard operations like matrix-vector products, resolution of linear systems and eigenvalues evaluations can be performed by means of FCT-III [18]

within  $O(n_1 n_2 \log(n_1 n_2))$  arithmetic operations (ops). For example, by multiplying by  $e_1 = [1, 0, \dots, 0]^T$  both the sides of  $R_n^T A_n = \Lambda_n R_n^T$ , it holds that

$$[\Lambda_n]_{(i_1, i_2)} = [R_n^T (A_n e_1)]_{(i_1, i_2)} / [R_n^T e_1]_{(i_1, i_2)}, \quad i_1 = 1, \dots, n_1, i_2 = 1, \dots, n_2,$$

i.e., it is enough to consider an inverse FCT-III applied to the first column of  $A_n$ , with a computational cost of  $O(n_1 n_2 \log(n_1 n_2))$  ops.

**2.2. ANTI-REFLECTIVE BOUNDARY CONDITIONS.** More recently, Anti-reflective boundary conditions (AR-BCs) have been proposed in [21] and studied [2, 3, 4, 9, 10, 19]. The improvement is due to the fact that not only the continuity of the image, but also of the normal derivative, are guaranteed at the boundary. This regularity, which is not shared with Dirichlet or periodic BCs, and only partially shared with reflective BCs, significantly reduces typical ringing artifacts.

The key idea is simply to assume that the scene outside the FOV is the anti-reflection of the scene inside the FOV. For example, with a boundary at  $x_1 = 0$  the anti-reflexive condition impose  $f(-x_1, x_2) - f(x_1^*, x_2) = -(f(x_1, x_2) - f(x_1^*, x_2))$ , for any  $x_2$ , where  $x_1^*$  is the center of the one-dimensional anti-reflection, i.e.,

$$f(-x_1, x_2) = 2f(x_1^*, x_2) - f(x_1, x_2), \text{ for any } x_2.$$

In order to preserve a tensorial structure, at the corners, a double anti-reflection, first with respect to one axis and after with respect to the other, is considered, so that the BCs impose

$$f(-x_1, -x_2) = 4f(x_1^*, x_2^*) - 2f(x_1^*, x_2) - 2f(x_1, x_2^*) + f(x_1, x_2),$$

where  $(x_1^*, x_2^*)$  is the center of the two-dimensional anti-reflection.

More precisely, by choosing as center of the anti-reflection the first available data, along the borders, the BCs impose

$$\begin{aligned} f_{1-i_1, i_2} &= 2f_{1, i_2} - f_{i_1+1, i_2}, & f_{n_1+i_1, i_2} &= 2f_{n_1, i_2} - f_{n_1-i_1, i_2}, & i_1 &= 1, \dots, q_1, & i_2 &= 1, \dots, n_2, \\ f_{i_1, 1-i_2} &= 2f_{i_1, 1} - f_{i_1, i_2+1}, & f_{i_1, n_2+i_2} &= 2f_{i_1, n_2} - f_{i_1, n_2-i_2}, & i_1 &= 1, \dots, n_1, & i_2 &= 1, \dots, q_2. \end{aligned}$$

At the corners, the BCs impose for any  $i_1 = 1, \dots, q_1$  and  $i_2 = 1, \dots, q_2$ ,

$$\begin{aligned} f_{1-i_1, 1-i_2} &= 4f_{1,1} - 2f_{1, i_2+1} - 2f_{i_1+1, 1} + f_{i_1+1, i_2+1}, \\ f_{1-i_1, n_2+i_2} &= 4f_{1, n_2} - 2f_{1, n_2-i_2} - 2f_{i_1+1, n_2} + f_{i_1+1, n_2-i_2}, \\ f_{n_1+i_1, 1-i_2} &= 4f_{n_1, 1} - 2f_{n_1, i_2+1} - 2f_{n_1-i_1, 1} + f_{n_1-i_1, i_2+1}, \\ f_{n_1+i_1, n_2+i_2} &= 4f_{n_1, n_2} - 2f_{n_1, n_1-i_2} - 2f_{n_1-i_1, n_2} + f_{n_1-i_1, n_2-i_2}. \end{aligned}$$

As a consequence the rectangular matrix  $\tilde{A}$  is reduced to a square Toeplitz-plus-Hankel block matrix with Toeplitz-plus-Hankel blocks, plus an additional structured low rank matrix.

Moreover, under the assumption of strong symmetry of the PSF and of a mild finite support condition (more precisely  $h_i = 0$  if  $|i_j| \geq n - 2$ , for some  $j \in \{1, 2\}$ ), the resulting linear system  $A_n f = g$  is such that  $A_n$  belongs to the  $\mathcal{AR}_n^{2D}$  commutative matrix algebra [3]. This new algebra shares some properties with the  $\tau$  (or DST-I) algebra [7].

Going inside the definition, a matrix  $A_n \in \mathcal{AR}_n^{2D}$  has the following block structure

$$A_n = \left[ \begin{array}{c|c|c} D_0 + Z^{[1]} & 0^T & 0 \\ \hline D_1 + Z^{[2]} & & 0 \\ \vdots & & \vdots \\ D_{q_1-1} + Z^{[q_1]} & & 0 \\ D_{q_1} & \tau(D_0, \dots, D_{q_1}) & D_{q_1} \\ 0 & & D_{q_1-1} + Z^{[q_1]} \\ \vdots & & \vdots \\ 0 & & D_1 + Z^{[2]} \\ \hline 0 & 0^T & D_0 + Z^{[1]} \end{array} \right],$$

where  $\tau(D_0, \dots, D_{q_1})$  is a block  $\tau$  matrix with respect to the  $\mathcal{AR}^{1D}$  blocks  $D_{i_1}$ ,  $i_1 = 1, \dots, q_1$  and  $Z^{[k]} = 2 \sum_{t=k}^{q_1} D_t$  for  $k = 1, \dots, q_1$ . In particular, the  $\mathcal{AR}^{1D}$  block  $D_{i_1}$  is associated to  $i_1^{\text{th}}$  row of the PSF, i.e.,  $h_{i_1}^{[1D]} = [h_{i_1, i_2}]_{i_2 = -q_2, \dots, q_2}$  and it is defined as

$$D_{i_1} = \left[ \begin{array}{c|c|c} h_{i_1,0} + z_{i_1}^{[1]} & 0^T & 0 \\ \hline h_{i_1,1} + z_{i_1}^{[2]} & & 0 \\ \vdots & & \vdots \\ h_{i_1, q_2-1} + z_{i_1}^{[q_2]} & & 0 \\ h_{i_1, q_2} & \tau(h_{i_1,0}, \dots, h_{i_1, q_2}) & h_{i_1, q_2} \\ 0 & & h_{i_1, q_2-1} + z_{i_1}^{[q_2]} \\ \vdots & & \vdots \\ 0 & & h_{i_1,1} + z_{i_1}^{[2]} \\ \hline 0 & 0^T & h_{i_1,0} + z_{i_1}^{[1]} \end{array} \right],$$

where  $z_{i_1}^{[k]} = 2 \sum_{t=k}^{q_2} h_{i_1, t}$  for  $k = 1, \dots, q_2$  and  $\tau(h_{i_1,0}, \dots, h_{i_1, q_2})$  is the unilevel  $\tau$  matrix associated to the one-dimensional PSF  $h_{i_1}^{[1D]}$  previously defined.

Notice that the rank-1 correction given by the elements  $z_{i_1}^{[k]}$  pertains to the contribution of the anti-reflection centers with respect to the vertical borders, while the low rank correction given by the matrices  $Z^{[k]}$  pertains to the contribution of the anti-reflection centers with respect to the horizontal borders.

It is evident from the above matrix structure that favorable computational properties are guaranteed also by virtue of the  $\tau$  structure. Therefore, firstly we recall the relevant properties of the two-level  $\tau$  algebra [7].

Let  $\mathcal{T}_n = \{A_n \in \mathbb{R}^{N(n) \times N(n)}, n = (n_1, n_2), N(n) = n_1 n_2 \mid A_n = Q_n \Lambda_n Q_n\}$  be the two-level  $\tau$  matrix algebra, i.e., the algebra of matrices that are simultaneously diagonalized by the symmetric orthogonal transform

$$Q_n = Q_{n_1} \otimes Q_{n_2}, \quad Q_m = \left[ \sqrt{\frac{2}{m+1}} \sin \left\{ \frac{st\pi}{m+1} \right\} \right]_{s,t=1}^m. \quad (2.3)$$

With the same notation as the DCT-III algebra case, the explicit structure of the matrix is two level Toeplitz-plus-Hankel. More precisely,

$$A_n = \text{Toeplitz}(V) - \text{Hankel}(\sigma^2(V), J\sigma^2(V))$$

with  $V = [V_0 \ V_1 \ \dots \ V_{q_1} \ 0 \ \dots \ 0]$ , where each  $V_{i_1}$ ,  $i_1 = 1, \dots, q_1$  is a the unilevel  $\tau$  matrix associated to the  $i_1^{th}$  row of the PSF mask, i.e.,  $V_{i_1} = \text{Toeplitz}(v_{i_1}) - \text{Hankel}(\sigma^2(v_{i_1}), J\sigma^2(v_{i_1}))$  with  $v_{i_1} = [h_{i_1,0}, \dots, h_{i_1,q_2}, 0, \dots, 0]$ . Here, we denote by  $\sigma^2$  the double shift operator such that  $\sigma^2(v_{i_1}) = [h_{i_1,2}, \dots, h_{i_1,q_2}, 0, \dots, 0]$ ; at the block level the same operations are intended in block-wise sense.

Once more, the spectral characterization is completely known since for any  $A_n \in \mathcal{T}_n$  the related eigenvalues are given by

$$\lambda_s(A_n) = f\left(x_{s_1}^{[n_1]}, x_{s_2}^{[n_2]}\right), s = (s_1, s_2), \quad x_r^{[m]} = \frac{r\pi}{m+1},$$

where  $s_1 = 1, \dots, n_1$ ,  $s_2 = 1, \dots, n_2$ , and  $f$  is the bivariate generating function associated to the  $PSF$  defined in (2.2).

As in the DCT-III case, standard operations like matrix-vector products, resolution of linear systems and eigenvalues evaluations can be performed by means of FST-I within  $O(n_1 n_2 \log(n_1 n_2))$  (ops). For instance, it is enough to consider a FST-I applied to the first column of  $A_n$  to obtain the eigenvalues

$$[\Lambda_n]_{(i_1, i_2)} = [Q_n(A_n e_1)]_{(i_1, i_2)} / [Q_n e_1]_{(i_1, i_2)}, \quad i_1 = 1, \dots, n_1, i_2 = 1, \dots, n_2.$$

Now, with respect to the  $\mathcal{AR}_n^{2D}$  matrix algebra, a complete spectral characterization is given in [3, 4]. A really useful fact is the existence of a transform  $T_n$  that simultaneously diagonalizes all the matrices belonging to  $\mathcal{AR}_n^{2D}$ , although the orthogonality property is partially lost.

**THEOREM 2.1.** [4] *Any matrix  $A_n \in \mathcal{AR}_n^{2D}$ ,  $n = (n_1, n_2)$ , can be diagonalized by  $T_n$ , i.e.,*

$$A_n = T_n \Lambda_n \tilde{T}_n, \quad \tilde{T}_n = T_n^{-1}$$

where  $T_n = T_{n_1} \otimes T_{n_2}$ ,  $\tilde{T}_n = \tilde{T}_{n_1} \otimes \tilde{T}_{n_2}$ , with

$$T_m = \begin{bmatrix} \alpha_m^{-1} & 0^T & 0 \\ \alpha_m^{-1} p & Q_{m-2} & \alpha_m^{-1} J p \\ 0 & 0^T & \alpha_m^{-1} \end{bmatrix} \quad \text{and} \quad \tilde{T}_m = \begin{bmatrix} \alpha_m & 0^T & 0 \\ -Q_{m-2} p & Q_{m-2} & -Q_{m-2} J p \\ 0 & 0^T & \alpha_m \end{bmatrix}$$

The entries of the vector  $p \in \mathbb{R}^{m-2}$  are defined as  $p_j = 1 - j / (m - 1)$ ,  $j = 1, \dots, m - 2$ ,  $J \in \mathbb{R}^{m-2 \times m-2}$  is the flip matrix, and  $\alpha_m$  is a normalizing factor chosen such that the Euclidean norm of the first and last column of  $T_m$  will be equal to 1.

**THEOREM 2.2.** [3] *Let  $A_n \in \mathcal{AR}_n^{2D}$ ,  $n = (n_1, n_2)$ , the matrix related to the PSF  $h_{PSF} = [h_{i_1, i_2}]_{i_1=-q_1, \dots, q_1, i_2=-q_2, \dots, q_2}$ . Then, the eigenvalues of  $A_n$  are given by*

- 1 with algebraic multiplicity 4,
- the  $n_2 - 2$  eigenvalues of the unilevel  $\tau$  matrix related to the one-dimensional PSF  $h^{\{r\}} = [\sum_{i_1=-q_1}^{q_1} h_{i_1, -q_2}, \dots, \sum_{i_1=-q_1}^{q_1} h_{i_1, q_2}]$ , each one with algebraic multiplicity 2,
- the  $n_1 - 2$  eigenvalues of the unilevel  $\tau$  matrix related to the one-dimensional PSF  $h^{\{c\}} = [\sum_{i_2=-q_2}^{q_2} h_{-q_1, i_2}, \dots, \sum_{i_2=-q_2}^{q_2} h_{q_1, i_2}]$ , each one with algebraic multiplicity 2,
- the  $(n_1 - 2)(n_2 - 2)$  eigenvalues of the two-level  $\tau$  matrix related to the two-dimensional PSF  $h_{PSF}$ .

Notice that the three sets of multiple eigenvalues are exactly related to the type of low rank correction imposed by the BCs through the centers of the anti-reflections. More in detail, the eigenvalues of  $\tau_{n_2-2}(h^{\{r\}})$  and of  $\tau_{n_1-2}(h^{\{c\}})$  take into account the condensed PSF information considered along the horizontal and vertical borders respectively, while the eigenvalue equal to 1 takes into account the condensed information of the whole PSF at the four corners.

In addition, it is worth noticing that the spectral characterization can be completely described in terms of the generating function associated to the *PSF* defined in (2.2), simply by extending to 0 the standard  $\tau$  evaluation grid, i.e., it holds

$$\lambda_s(A_n) = f\left(x_{s_1}^{[n_1]}, x_{s_2}^{[n_2]}\right), s = (s_1, s_2), s_j = 0, \dots, n_j, \quad x_r^{[m]} = \frac{r\pi}{m+1},$$

where the 0-index refers to the first/last columns of the matrix  $T_m$  [3].

See [2, 4] for some algorithms related to standard operations like matrix-vector products, resolution of linear systems and eigenvalues evaluations with a computational cost of  $O(n_1 n_2 \log(n_1 n_2))$  ops.

It is worthwhile stressing that the computational cost of the inverse transform is comparable with that of the direct transform and, at least at first sight, the very true penalty is the loss of orthogonality due to the first/last column of the matrix  $T_m$ .

**3. FILTERING METHODS.** Owing to the ill-conditioning, the standard solution  $f = A_n^{-1}g$  is not physically meaningful since it is completely corrupted by the noise propagation from data to solution, i.e., by the so called inverted noise. For this reason, restoration methods look for an approximate solution with controlled noise levels: widely considered regularization methods are obtained through spectral filtering [14, 16]. Hereafter, we consider the truncated Singular Values Decompositions (SVDs) (or Spectral Decompositions (SDs)) and the Tikhonov (or Re-blurring) regularization method.

**3.1. TRUNCATED SVDs AND TRUNCATED SDs.** The Singular Values Decomposition (SVD) highlights a standard perspective for dealing with the inverted noise. More precisely, if

$$A_n = U_n \Sigma_n V_n^T \in \mathbb{R}^{N(n) \times N(n)}$$

is the SVD of  $A_n$ , i.e.,  $U_n$  and  $V_n$  are orthogonal matrices and  $\Sigma_n$  is a diagonal matrix with entries  $\sigma_1 \geq \sigma_2 \geq \dots \geq \sigma_{N(n)} \geq 0$ , then the solution of the linear system  $A_n f = g$  can be written as

$$f = \sum_{k=1}^{N(n)} \left( \frac{u_k^T g}{\sigma_k} \right) v_k,$$

where  $u_k$  and  $v_k$  denote the  $k^{\text{th}}$  column of the matrix  $U_n$  and  $V_n$ , respectively.

With regard to the image restoration problem, the idea is to consider a sharp filter, i.e., to take in the summation only the terms corresponding to singular values greater than a certain threshold value  $\delta$ , so damping the effects caused by division by the small singular values. Therefore, by setting the filter factors as

$$\phi_k = \begin{cases} 1, & \text{if } \sigma_k \geq \delta, \\ 0, & \text{otherwise,} \end{cases}$$

the filtered solution is defined as

$$f_{\text{filt}} = \sum_{k=1}^{N(n)} \left( \phi_k \frac{u_k^T g}{\sigma_k} \right) v_k = \sum_{k \in I_\delta} \left( \phi_k \frac{u_k^T g}{\sigma_k} \right) v_k, \quad I_\delta = \{k \mid \sigma_k \geq \delta\}.$$

Due to scale of the problem, the SVD of the matrix  $A_n$  is in general an expensive computational task (and not negligible also in the case of a separable PSF). Thus, an ‘‘a priori’’ known spectral decomposition, whenever available, can give rise to a valuable simplification. More precisely, let

$$A_n = V_n \Lambda_n \tilde{V}_n \in \mathbb{R}^{N(n) \times N(n)}, \quad \tilde{V}_n = V_n^{-1}$$

be a spectral decomposition of  $A_n$ , then the filtered solution is defined as

$$f_{\text{filt}} = \sum_{k=1}^{N(n)} \left( \phi_k \frac{\tilde{v}_k g}{\lambda_k} \right) v_k = \sum_{k \in I_\delta} \left( \phi_k \frac{\tilde{v}_k g}{\lambda_k} \right) v_k, \quad I_\delta = \{k \mid |\lambda_k(A)| \geq \delta\},$$

where  $v_k$  and  $\tilde{v}_k$  denote the  $k^{\text{th}}$  column of  $V_n$  and the  $k^{\text{th}}$  row of  $\tilde{V}_n$ , respectively, and where  $\phi_k = 1$  if  $k \in I_\delta$ , 0 otherwise.

**3.2. TIKHONOV AND RE-BLURRING REGULARIZATIONS.** In the classical Tikhonov regularization method, the image filtering is obtained by looking for the solution of the following minimization problem

$$\min_f \|A_n f - g\|_2^2 + \mu \|D_n f\|_2^2, \quad (3.1)$$

where  $\mu > 0$  is the regularization parameter and  $D_n$  is a carefully chosen matrix (typically  $D_n = I_n$  or represents the discretization of a differential operator, properly adapted with respect to the chosen BCs).

The target is to minimize the Euclidean norm of the residual  $\|A_n f - g\|_2$  without explosions with respect to the quantity  $\|D_n x\|_2$ . As well know, (3.1) is equivalent to the solution to the damped least square problem

$$(A_n^T A_n + \mu D_n^T D_n) f = A_n^T g. \quad (3.2)$$

In addition, the regularization Tikhonov method can be reinterpreted in the framework of classical spectral filtering method. For instance, in the case of  $D_n = I_n$ , by making use of the SVD of  $A_n = U_n \Sigma_n V_n^T$ , the solution of (3.2) can be rewritten as

$$f_{\text{filt}} = V_n \Phi_n \Sigma_n^{-1} U_n^T g,$$

where  $\Phi_n = \text{diag}(\phi_k)$  with  $\phi_k = \sigma_k^2 / (\sigma_k^2 + \mu)$ ,  $k = 1, \dots, N(n)$ .

A severe drawback in adopting the Tikhonov regularization approach in the case of  $A_n \in \mathcal{AR}_n^{2D}$  is due to the fact that  $A_n^T \notin \mathcal{AR}_n^{2D}$ , so that all the favorable computational properties are substantially spoiled. An alternative approach, named Re-blurring, has been proposed in [11, 9]: the proposal is to replace  $A_n^T$  by  $A'_n$  in (3.2), where  $A'_n$  is the blurring matrix related to the current BCs with a PSF rotated by  $180^\circ$ . This approach is completely equivalent to (3.2) in the case of Dirichlet and Periodic BCs, while the novelty concerns both Reflective BCs and Anti-Reflective

BCs, where in general  $A'_n \neq A_n^T$ . The authors show that the Re-blurring with anti-reflective BCs is computationally convenient and leads to a larger reduction of the ringing effects arising in classical deblurring schemes. From the modelling point of view, the authors motivation relies upon the fact that Re-blurring smoothes the noise in the right hand side of the system, in the same manner as this happens in the case of Dirichlet, Periodic and Reflective BCs.

Hereafter, we consider an explanation of the observed approximation results. As previously claimed, we focus our attention on the case of a strongly symmetric PSF, so that the matrix  $A'_n$  equals the matrix  $A_n$ . Moreover, also in this case it is evident that the linear system

$$(A_n^2 + \mu D_n^2)f = A_n g. \quad (3.3)$$

is not equivalent to a minimization problem, again because the matrix  $A \in \mathcal{AR}_n^{2D}$  is not symmetric. Nevertheless, the symmetrization of (3.3) can be performed by diagonalization, so obtaining

$$(\Lambda_{A,n}^2 + \mu \Lambda_{D,n}^2)\hat{f} = \Lambda_{A,n}\hat{g}, \quad (3.4)$$

where  $\hat{f} = \tilde{T}_n f$  and  $\hat{g} = \tilde{T}_n g$ . In such a way (3.4) is again equivalent to the minimization problem

$$\min_f \|\Lambda_{A,n}\tilde{T}_n f - \tilde{T}_n g\|_2^2 + \mu \|\Lambda_{D,n}\tilde{T}_n f\|_2^2, \quad (3.5)$$

or equivalently, again by making use of the diagonalization result, to

$$\min_f \|\tilde{T}_n(A_n f - g)\|_2^2 + \mu \|\tilde{T}_n D_n f\|_2^2. \quad (3.6)$$

Clearly, the last formulation in (3.6) is the most natural and it allows to claim that the Re-blurring method can be interpreted as a standard Tikhonov regularization method in the space transformed by means of  $\tilde{T}_n$ .

Recalling that  $\tilde{T}_n$  is not an orthogonal transformation, the goal becomes to compare  $\|\tilde{T}_n f\|_2$  and  $\|f\|_2$ , that is to bound  $\|\tilde{T}_n\|_2 = \|\tilde{T}_{n_1}\|_2 \|\tilde{T}_{n_2}\|_2$ , being  $\|\tilde{T}_n f\|_2 \leq \|\tilde{T}_n\|_2 \|f\|_2$ .

A quite sharp estimate of such a norm can be found by exploiting the structure of the unilevel matrix  $\tilde{T}_m \in \mathbb{R}^{m \times m}$ . Let  $\check{f} = [f_2, \dots, f_{m-1}]$ , it holds that

$$\begin{aligned} \|\tilde{T}_m f\|_2^2 &= \alpha_m^2 f_1^2 + \|Q_{m-2}(-f_1 p + \check{f} - f_n J p)\|_2^2 + \alpha_m^2 f_m^2 \\ &= \alpha_m^2 (f_1^2 + f_m^2) + \|-f_1 p + \check{f} - f_n J p\|_2^2 \\ &\leq \alpha_m^2 (f_1^2 + f_m^2) + (\|\check{f}\|_2 + (|f_1| + |f_n|)\|p\|_2)^2 \\ &\leq \alpha_m^2 (f_1^2 + f_m^2) + \|\check{f}\|_2^2 + 3\|p\|_2^2 \|f\|_2^2 + 4\|p\|_2 \|f\|_2^2 \\ &\leq (1 + 2\|p\|_2)^2 \|f\|_2^2, \end{aligned}$$

being  $\alpha_m^2 = 1 + \|p\|_2^2$ . Since, by definition,  $\|p\|_2^2 \simeq m$ , we have

$$\|\tilde{T}_m\|_2 \leq 1 + 2\|p\|_2 \simeq 2\sqrt{m}. \quad (3.7)$$

Notice that the bound given in (3.7) is quite sharp, since for instance  $\|\tilde{T}_m e_1\|_2^2$  equals  $1 + 2\|p\|_2^2$ .

**4. CROSS-CHANNEL BLURRING.** Hereafter, we extend the analysis of the deblurring problem to the case of color images digitalized, for instance, according to the standard RGB system. Several techniques can be used for recording color images, but the main problem concerns the fact that light from one color channel can end up on a pixel assigned to another color. The consequence of this phenomenon is called cross-channel blurring among the three channels of the image and it sums up to the previously analyzed blurring of each one of the three colors, named within-channel blurring.

By assuming that the cross-channel blurring takes place after the within-channel blurring of the image, that it is spatially invariant and by assuming that the same within-channel blurring occurs in all the three color channels, the problem can be modelled [16] as

$$(A_{\text{color}} \otimes A_n)f = g - \eta \quad (4.1)$$

with  $A_n \in \mathbb{R}^{N(n) \times N(n)}$ ,  $n = (n_1, n_2)$ ,  $N(n) = n_1 n_2$ , and

$$A_{\text{color}} = \begin{bmatrix} a_{rr} & a_{rg} & a_{rb} \\ a_{gr} & a_{gg} & a_{gb} \\ a_{br} & a_{bg} & a_{bb} \end{bmatrix}.$$

The row-entries denote the amount of within-channel blurring pertaining to each color channel; a normalized conservation law prescribes that  $A_{\text{color}}e = e$ ,  $e = [1 \ 1 \ 1]^T$ . Lastly, the vectors  $f, g, \eta \in \mathbb{R}^{3N(n)}$  are assumed to collect the three color channels in the RGB order.

Clearly, if  $A_{\text{color}} = I_3$ , i.e., the blurring is only of within-channel type, the problem is simply decoupled into three independent gray-scale deblurring problems.

In the general case, taking into account the tensorial structure of the whole blurring matrix  $A_{\text{color}} \otimes A_n$  is evident that the truncated SVDs and SDs can be formulated as the natural extension of those considered in the within-blurring case. Notice that in the case of SDs, we will consider a SVD for the matrix  $A_{\text{color}}$ , since it naturally assures an orthogonal decomposition, no matter about the specific matrix, while its computational cost is negligible with respect to the scale of the problem. In addition, we tune the filtering strategy with respect the spectral information given only by the matrix  $A_n$ , i.e., for any fixed  $\sigma_k$  (or  $\lambda_k$ ) we simultaneously sum, or discard, the three contribution on  $f$  related to the three singular values of  $A_{\text{color}}$ .

With respect to the Tikhonov regularization method, the approach is a bit more involved. Under the assumption  $A_n = A_n^T = V_n \Lambda_n \tilde{V}_n$ , the damped least square problem

$$[(A_{\text{color}} \otimes A_n)^T (A_{\text{color}} \otimes A_n) + \mu I_{3n}]f = (A_{\text{color}} \otimes A_n)^T g$$

can be rewritten as

$$[(A_{\text{color}}^T A_{\text{color}}) \otimes V_n \Lambda_n^2 \tilde{V}_n + \mu(I_3 \otimes I_n)]f = (A_{\text{color}} \otimes V_n \Lambda_n \tilde{V}_n)^T g. \quad (4.2)$$

Thus, by setting  $S_{3n} = I_3 \otimes \tilde{V}_n$ ,  $\hat{f} = S_{3n}f$ ,  $\hat{g} = S_{3n}g$ , (4.2) can be transformed in

$$S_{3n}[(A_{\text{color}}^T A_{\text{color}}) \otimes V_n \Lambda_n^2 \tilde{V}_n + \mu(I_3 \otimes I_n)]S_{3n}^{-1}\hat{f} = S_{3n}(A_{\text{color}} \otimes V_n \Lambda_n \tilde{V}_n)^T S_{3n}^{-1}\hat{g},$$

so obtaining the linear system

$$[(A_{\text{color}}^T A_{\text{color}}) \otimes \Lambda_n^2 + \mu(I_3 \otimes I_n)]\hat{f} = (A_{\text{color}}^T \otimes \Lambda_n)\hat{g},$$

that can easily be decoupled into  $n_1 n_2$  linear systems of dimension 3.

Clearly, in the case of any matrix  $A_n \in \mathcal{C}_n$ , all these manipulations can be performed by means of an orthogonal transformation  $S_{3n}$ . Notice also that the computational cost is always  $O(n_1 n_2 \log n_1 n_2)$  ops.

With respect to  $A_n = T_n \Lambda_n \tilde{T}_n \in \mathcal{AR}_n^{2D}$ , we can consider the same strategy by referring to the Re-blurring regularization method. More precisely, the linear system

$$[(A_{\text{color}}^T A_{\text{color}}) \otimes A_n^2 + \mu(I_3 \otimes I_n)]f = (A_{\text{color}}^T \otimes A_n)g$$

can be transformed in

$$[(A_{\text{color}}^T A_{\text{color}}) \otimes \Lambda_n^2 + \mu(I_3 \otimes I_n)]\hat{f} = (A_{\text{color}}^T \otimes \Lambda_n)\hat{g}.$$

Though the transformation  $S_{3n} = I_3 \otimes \tilde{T}_n$  is not orthogonal as in the Reflective case, the obtained restored image are fully comparable with the previous ones and the computational cost is still  $O(n_1 n_2 \log n_1 n_2)$  ops.

## 5. NUMERICAL TESTS.

**5.1. SOME COMPUTATIONAL ISSUES.** Before analyzing the image restoration results, we discuss how the methods can work without reshaping the involved data. In fact, the tensorial structure of the matrices, obtained by considering Reflective and Anti-Reflective BCs, can be exploited in depth, so that the algorithms can deal directly, and more naturally, with the data collected in matrix form. Hereafter, we consider a two-index notation in the sense of the previously adopted row-wise ordering.

In the SD case considered in Section 3.1, since  $\tilde{v}_k = \tilde{v}_{k_1}^{[n_1]} \otimes \tilde{v}_{k_2}^{[n_2]}$  is represented in matrix form as  $(\tilde{v}_{k_1}^{[n_1]})^T \tilde{v}_{k_2}^{[n_2]}$ , the required scalar product can be computed as

$$\tilde{v}_k g = \left[ \left( \tilde{v}_{k_1}^{[n_1]} \right)^T \tilde{v}_{k_2}^{[n_2]} \right] \odot G,$$

where  $\odot$  denotes the summation of all the involved terms after a element-wise product. Clearly,  $v_k = v_{k_1}^{[n_1]} \otimes v_{k_2}^{[n_2]}$  is represented in matrix form as  $v_{k_1}^{[n_1]} (\tilde{v}_{k_2}^{[n_2]})^T$ . In a similar manner, in the case of the SVD of  $A_n$  with separable PSF  $h = h_1 \otimes h_2$ , we can represent  $v_k = v_{k_1}^{[n_1]} \otimes v_{k_2}^{[n_2]}$  in matrix form as  $v_{k_1}^{[n_1]} (v_{k_2}^{[n_2]})^T$  and  $u_k^T = (u_{k_1}^{[n_1]} \otimes u_{k_2}^{[n_2]})^T$  as  $u_{k_1}^{[n_1]} (u_{k_2}^{[n_2]})^T$ .

The eigenvalues required for the SD can be stored into a matrix  $\Lambda^* \in \mathbb{R}^{n_1 \times n_2}$ . In the case of  $A_n \in \mathcal{C}_n$  this matrix can be evaluated as

$$\Lambda^* = \left( \tilde{V}_{n_2} A^* \tilde{V}_{n_1}^T ./ \tilde{V}_{n_2} E_1^* \tilde{V}_{n_1}^T \right)^T$$

where  $A^* \in \mathbb{R}^{n_2 \times n_1}$  denotes the first column of  $A_n$  and  $E_1^*$  the first canonical basis vector, reshaped as matrices in column-wise order. In addition, the two-level direct and inverse transform  $y = V_n x$  and  $y = \tilde{V}_n x$  can be directly evaluated on a matrix data as

$$Y = V_{n_1} X V_{n_2}^T = (V_{n_2} (V_{n_1} X)^T)^T \quad \text{and} \quad Y = \tilde{V}_{n_1} X \tilde{V}_{n_2} = (\tilde{V}_{n_2} (\tilde{V}_{n_1} X)^T)^T$$

by referring to the corresponding unilevel transforms.

In the same way, the eigenvalues required in the case of  $A_n \in \mathcal{AR}_n^{2D}$  can be suitably

stored as

$$\Lambda^* = \left[ \begin{array}{c|c|c} 1 & \Lambda^*(\tau_{n_2-2}(h^r)) & 1 \\ \hline \Lambda^*(\tau_{n_1-2}(h^c)) & \Lambda^*(\tau_{n-2}(h)) & \Lambda^*(\tau_{n_1-2}(h^c)) \\ \hline 1 & \Lambda^*(\tau_{n_2-2}(h^r)) & 1 \end{array} \right] \in \mathbb{R}^{n_1 \times n_2},$$

with reference to the notations of Theorem 2.2, where the eigenvalues of the unilevel and two-level  $\tau$  matrices are evaluated as outlined in Section 2.2.

Lastly, the linear systems obtained, for any fixed  $\mu$ , in the case of Tikhonov and Re-blurring regularization methods can be solved with reference to the matrix  $\Phi_n$  of the corresponding filter factors by applying the Reflective and Anti-Reflective transforms with a computational cost  $O(n_1 n_2 \log n_1 n_2)$  ops.

**5.2. TRUNCATED DECOMPOSITIONS.** In this section we compare the effectiveness of truncated spectral decompositions (SDs) with respect to the standard truncated SVDs both in the case of Reflective and Anti-Reflective BCs. Due to scale of the problem, the SVD of the matrix  $A_n$  is in general an expensive computational task (and not negligible also in the case of a separable PSF). Thus, a spectral decomposition, whenever available as in these cases, leads to a valuable simplification. Firstly, we consider the case of the separable PSF caused by atmospheric turbulence

$$h_{i_1, i_2} = \frac{1}{2\pi\sigma_{i_1}\sigma_{i_2}} \exp\left(-\frac{1}{2}\left(\frac{i_1}{\sigma_{i_1}}\right)^2 - \frac{1}{2}\left(\frac{i_2}{\sigma_{i_2}}\right)^2\right),$$

where  $\sigma_{i_1}$  and  $\sigma_{i_2}$  determine the width of the PSF itself. Since the Gaussian function decays exponentially away from its center, it is customary to truncate the values in the PSF mask after an assigned decay  $|i_1|, |i_2| \leq l$ . It is evident from the quoted definition that the Gaussian PSF satisfies the strong symmetry condition (1.7). Another example of strongly symmetric PSF is given by the PSF representing the out-of-focus blur

$$h_{i_1, i_2} = \begin{cases} \frac{1}{\pi r^2}, & \text{if } i_1^2 + i_2^2 \leq r^2, \\ 0, & \text{otherwise,} \end{cases}$$

where  $r$  is the radius of the PSF.

In the reported numerical tests, the blurred image  $g$  has been perturbed by adding a Gaussian noise contribution  $\eta = \eta_n \nu$  with  $\nu$  fixed noise vector,  $\eta_n = \rho \|g\|_2 / \|\nu\|_2$ , and  $\rho$  assigned value. In such a way the Signal Noise Ratio (SNR) [5] is given by

$$SNR = 20 \log_{10} \frac{\|g\|_2}{\|\eta\|_2} = 20 \log_{10} \rho^{-1} \text{ (dB)}.$$

### 5.2.1. GRAY-SCALE IMAGES.

In Figure 5.1 we report the template true image (the FOV is delimited by a white frame), together with the blurred image with the Gaussian PSF with support  $15 \times 15$  and  $\sigma_{i_1} = \sigma_{i_2} = 2$  and the reference perturbation  $\nu$ , reshaped in matrix form.

We consider the optimal image restoration with respect to the relative restoration error (RRE), i.e.,  $\|f_{\text{filt}} - f_{\text{true}}\|_2 / \|f_{\text{true}}\|_2$ , where  $f_{\text{filt}}$  is the computed approximation

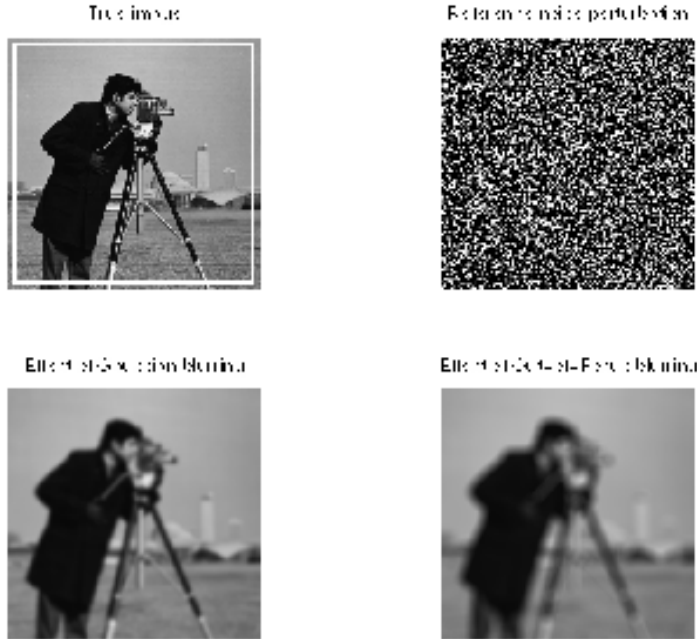


FIG. 5.1. *True image (FOV is delimited by a white frame), reference noise perturbation, blurred image with the Gaussian PSF with support  $15 \times 15$  and  $\sigma_{i_1} = \sigma_{i_2} = 2$ , and blurred image with the Out-of-Focus PSF with support  $15 \times 15$ .*

of the true image  $f_{\text{true}}$  by considering spectral filtering. More in detail, the RRE is analyzed by progressively adding a new basis element at a time, according to the non-decreasing order of the singular/eigen-values (the eigenvalues are ordered with respect to their absolute value).

In the case of SDs (or SVDs related to a separable PSF) this can be done as described in Section 5.1 and, beside the preliminary cost related to the decomposition computation, the addition of a new term has a computational cost equal to  $4n_1n_2$  ops. The algorithm proposed in [4], that makes use of the Anti-Reflective direct and inverse transforms, is less expensive in the case of tests with few threshold values.

Hereafter, the aim is to compare the truncated SVD with the truncated SD restorations both in the case of Reflective and Anti-Reflective BCs. Periodic BCs are not analyzed here, since Reflective and Anti-Reflective BCs give better performances with respect to the approximation of the image at the boundary.

In Table 5.1 and 5.2 we report the results obtained by varying the dimension of the PSF support, the parameter  $\rho$  related to the amount of the noise perturbation and the variance of the considered Gaussian blur. As expected the optimal RRE worses as the parameter  $\rho$  increases and the Anti-Reflective BCs show better performances in the case of low noise levels. In fact, for low  $\rho$  values, the reduction of ringing artifacts is significant, while the quality of the restoration for higher  $\rho$  values is essentially driven by the goal of noise filtering. Therefore, in such a case, the choice of the BCs becomes more and more meaningless since it is not able to influence the image restora-

TABLE 5.1

Optimal RREs of truncated SVD and SD with reference to the true image in Figure 5.1 (Gaussian blur  $\sigma_{i_1} = \sigma_{i_2} = 2$ ).

| Reflective BCs |          |          |          |          | Anti-Reflective BCs |          |          |          |          |
|----------------|----------|----------|----------|----------|---------------------|----------|----------|----------|----------|
| PSF            | 5x5      | 11x11    | 15x15    | 21x21    | PSF                 | 5x5      | 11x11    | 15x15    | 21x21    |
| $\rho = 0$     |          |          |          |          | $\rho = 0$          |          |          |          |          |
| SVD            | 0.059164 | 0.087402 | 0.090742 | 0.093856 | SVD                 | 0.039165 | 0.064081 | 0.086621 | 0.087237 |
| SD             | 0.043754 | 0.087400 | 0.090746 | 0.093867 | SD                  | 0.038316 | 0.063114 | 0.083043 | 0.083521 |
| $\rho = 0.001$ |          |          |          |          | $\rho = 0.001$      |          |          |          |          |
| SVD            | 0.060278 | 0.091964 | 0.094468 | 0.097034 | SVD                 | 0.062182 | 0.094237 | 0.098897 | 0.10042  |
| SD             | 0.060278 | 0.091964 | 0.094476 | 0.097034 | SD                  | 0.059617 | 0.089105 | 0.092814 | 0.094343 |
| $\rho = 0.01$  |          |          |          |          | $\rho = 0.01$       |          |          |          |          |
| SVD            | 0.091151 | 0.11214  | 0.11307  | 0.11495  | SVD                 | 0.096049 | 0.12231  | 0.12403  | 0.12536  |
| SD             | 0.091152 | 0.11214  | 0.11307  | 0.11495  | SD                  | 0.091383 | 0.11230  | 0.11343  | 0.11495  |
| $\rho = 0.05$  |          |          |          |          | $\rho = 0.05$       |          |          |          |          |
| SVD            | 0.11635  | 0.13356  | 0.13508  | 0.13739  | SVD                 | 0.12791  | 0.15070  | 0.15188  | 0.15492  |
| SD             | 0.11635  | 0.13356  | 0.13510  | 0.13739  | SD                  | 0.11666  | 0.13414  | 0.13570  | 0.13816  |
| $\rho = 0.1$   |          |          |          |          | $\rho = 0.1$        |          |          |          |          |
| SVD            | 0.13024  | 0.14607  | 0.14746  | 0.15047  | SVD                 | 0.14399  | 0.16756  | 0.16964  | 0.17225  |
| SD             | 0.13024  | 0.14607  | 0.14746  | 0.15047  | SD                  | 0.13083  | 0.14709  | 0.14852  | 0.15162  |

TABLE 5.2

Optimal RREs of truncated SVD and SD with reference to the true image in Figure 5.1 (Gaussian blur  $\sigma_{i_1} = \sigma_{i_2} = 5$ ).

| Reflective BCs |          |          |          |         | Anti-Reflective BCs |          |          |          |         |
|----------------|----------|----------|----------|---------|---------------------|----------|----------|----------|---------|
| PSF            | 5x5      | 11x11    | 15x15    | 21x21   | PSF                 | 5x5      | 11x11    | 15x15    | 21x21   |
| $\rho = 0$     |          |          |          |         | $\rho = 0$          |          |          |          |         |
| SVD            | 0.063387 | 0.081274 | 0.097351 | 0.14634 | SVD                 | 0.040214 | 0.079543 | 0.088224 | 0.13686 |
| SD             | 0.045365 | 0.081274 | 0.096387 | 0.14634 | SD                  | 0.039437 | 0.078970 | 0.088832 | 0.13129 |
| $\rho = 0.001$ |          |          |          |         | $\rho = 0.001$      |          |          |          |         |
| SVD            | 0.063915 | 0.096243 | 0.11449  | 0.15217 | SVD                 | 0.068197 | 0.095808 | 0.11522  | 0.15767 |
| SD             | 0.063915 | 0.096274 | 0.11449  | 0.15217 | SD                  | 0.063575 | 0.093247 | 0.1127   | 0.14893 |
| $\rho = 0.01$  |          |          |          |         | $\rho = 0.01$       |          |          |          |         |
| SVD            | 0.089032 | 0.13343  | 0.14947  | 0.17397 | SVD                 | 0.09412  | 0.14482  | 0.16825  | 0.21148 |
| SD             | 0.089032 | 0.13343  | 0.14946  | 0.17397 | SD                  | 0.089038 | 0.13611  | 0.15270  | 0.17446 |
| $\rho = 0.05$  |          |          |          |         | $\rho = 0.05$       |          |          |          |         |
| SVD            | 0.12203  | 0.16002  | 0.17339  | 0.18335 | SVD                 | 0.13553  | 0.18563  | 0.21006  | 0.22962 |
| SD             | 0.12203  | 0.16002  | 0.17339  | 0.18335 | SD                  | 0.12253  | 0.16269  | 0.17439  | 0.18414 |
| $\rho = 0.1$   |          |          |          |         | $\rho = 0.1$        |          |          |          |         |
| SVD            | 0.13412  | 0.16793  | 0.17963  | 0.19057 | SVD                 | 0.15010  | 0.20164  | 0.22256  | 0.23960 |
| SD             | 0.13412  | 0.16793  | 0.17963  | 0.19057 | SD                  | 0.13487  | 0.16916  | 0.18088  | 0.19218 |

tion quality. Some examples of restored images are reported in Figure 5.2.

More impressive is the fact that SDs give better, or equal, results with respect to those obtained by considering SVDs. This numerical evidence is really interesting in the case of Anti-Reflective BCs: despite the loss of the orthogonality property in the spectral decomposition, the restoration results are better than those obtained by considering SVD. Moreover, the observed trend with respect to the Reflective BCs is also conserved.

A further analysis refers to the so-called Picard plots (see Figure 5.3), where the coefficients  $|u_k^T g|$ , or  $|\hat{v}_k g|$ , (black dots) are compared with the singular values  $\sigma_k$ , or the absolute values of the eigenvalues  $|\lambda_k|$ , (red line). As expected, initially these coefficients decrease faster than  $\sigma_k$ , or  $|\lambda_k|$ , while afterwards they level off at a plateau determined by the level of the noise in the image.

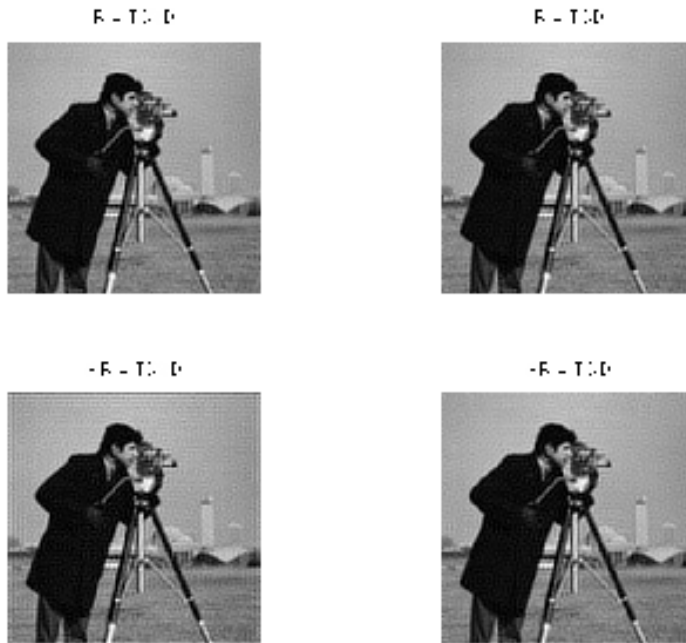
The threshold of this change of behavior is in good agreement with the optimal  $k$  value obtained in the numerical test by monitoring the RRE.

Moreover, notice that the Picard plots related to the SDs are quite in agreement with those corresponding to SVDs. In the case of the Anti-Reflective SD we observe an increasing data dispersion with respect to the plateau, but the correspondence between the threshold and the chosen optimal  $k$  is still preserved.

The computational relevance of this result is due to the significant lower computational cost required by the Anti-Reflective SDs with respect to the corresponding SVDs.

Lastly, Table 5.3 reports the spectral filtering results obtained in the case of Out-of-Focus blur by varying the dimension of the PSF support and the parameter  $\rho$  related

$$\rho = 0.01$$



$$\rho = 0.05$$

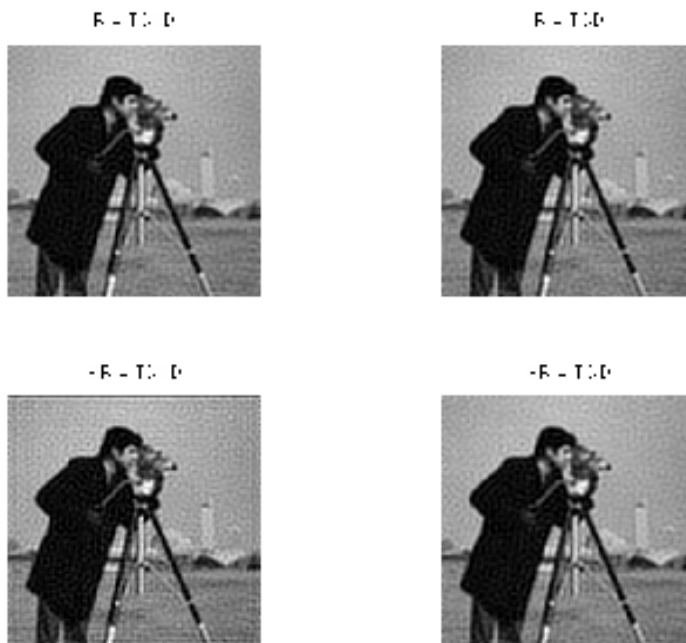


FIG. 5.2. Optimal restorations of truncated SVD and SD in the case of Reflective and Anti-Reflective BCs with reference to Figure 5.1 (Gaussian blur  $\sigma_{i_1} = \sigma_{i_2} = 2$ ).

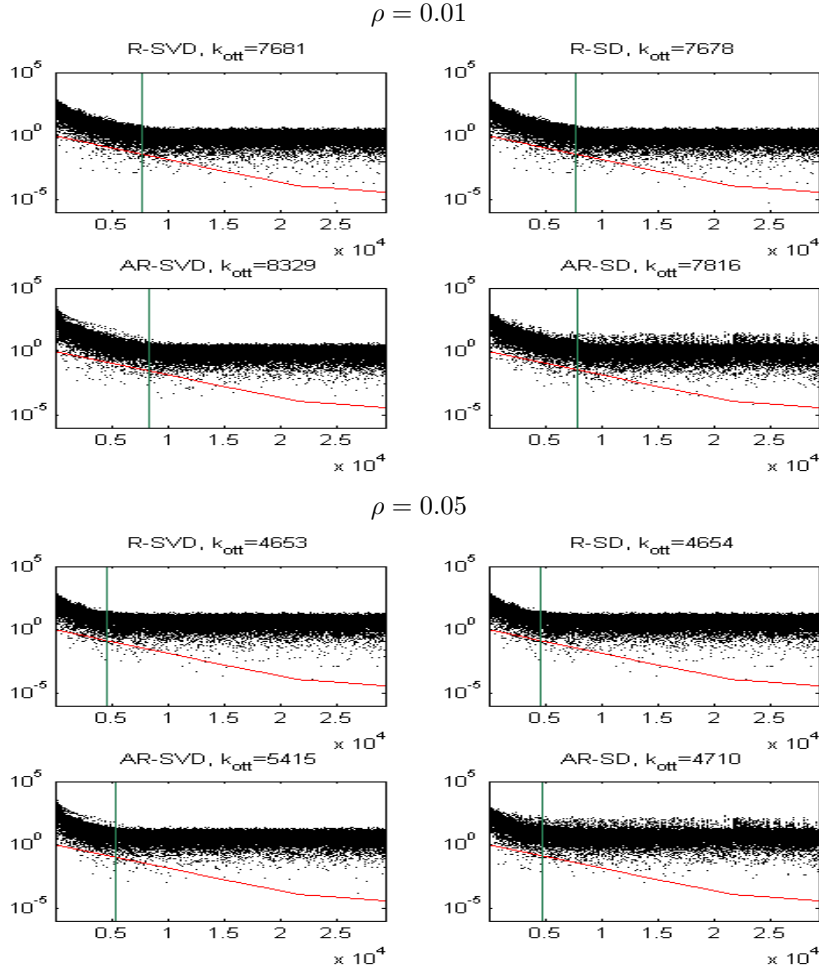


FIG. 5.3. Picard plot of truncated SVD and SD in the case of Reflective and Anti-Reflective BCs with reference to Figure 5.1 (Gaussian blur  $\sigma_{i_1} = \sigma_{i_2} = 2$ ).

TABLE 5.3

Optimal RREs of truncated SDs with reference to the true image in Figure 5.1 (Out-of-Focus blur).

| PSF            | Reflective BCs |          |          |          | Anti-Reflective BCs |          |          |          |
|----------------|----------------|----------|----------|----------|---------------------|----------|----------|----------|
|                | 5x5            | 11x11    | 15x15    | 21x21    | 5x5                 | 11x11    | 15x15    | 21x21    |
| $\rho = 0$     | 0.072593       | 0.084604 | 0.088323 | 0.096479 | 0.072821            | 0.085366 | 0.091252 | 0.099293 |
| $\rho = 0.001$ | 0.072671       | 0.085809 | 0.091035 | 0.10436  | 0.072904            | 0.086643 | 0.093929 | 0.10752  |
| $\rho = 0.01$  | 0.080016       | 0.12255  | 0.13569  | 0.15276  | 0.080427            | 0.12316  | 0.13803  | 0.15683  |
| $\rho = 0.05$  | 0.10645        | 0.15365  | 0.16810  | 0.18777  | 0.10685             | 0.15571  | 0.17147  | 0.19172  |
| $\rho = 0.1$   | 0.12089        | 0.16314  | 0.17836  | 0.20471  | 0.12147             | 0.16482  | 0.17987  | 0.20829  |

to the noise perturbation. The RRE follows the same trend observed in the case of Gaussian blur. Other image restoration tests with different gray-scale images have been considered in [20].

A more interesting remark again pertains the computational cost. Since the Out-of-Focus PSF is not separable, but the transforms are, the use of SDs related to Reflective or Anti-Reflective BCs allows to exploit the tensorial nature of the corresponding transforms, both with respect to the computation of the eigenvalues and of

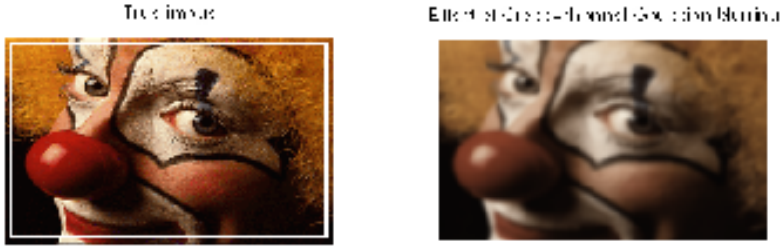


FIG. 5.4. True image (FOV is delimited by a white frame) and cross-channel blurred image with the Gaussian PSF with support  $15 \times 15$  and  $\sigma_{i_1} = \sigma_{i_2} = 2$  and matrix  $A_{\text{color}}$  in (5.1).

the eigenvectors (or of the Reflective and Anti-Reflective transforms).

**5.2.2. COLOR IMAGES IN THE CASE OF CROSS-CHANNEL BLURRING.** Here, we analyze some restoration tests in the case the template color image reported in Figure 5.4, by assuming the presence of a cross-channel blurring phenomenon modelled according to (4.1). The entity of this mixing effect is chosen according to the matrix

$$A_{\text{color}} = \begin{bmatrix} 0.7 & 0.2 & 0.1 \\ 0.25 & 0.5 & 0.25 \\ 0.15 & 0.1 & 0.75 \end{bmatrix}. \quad (5.1)$$

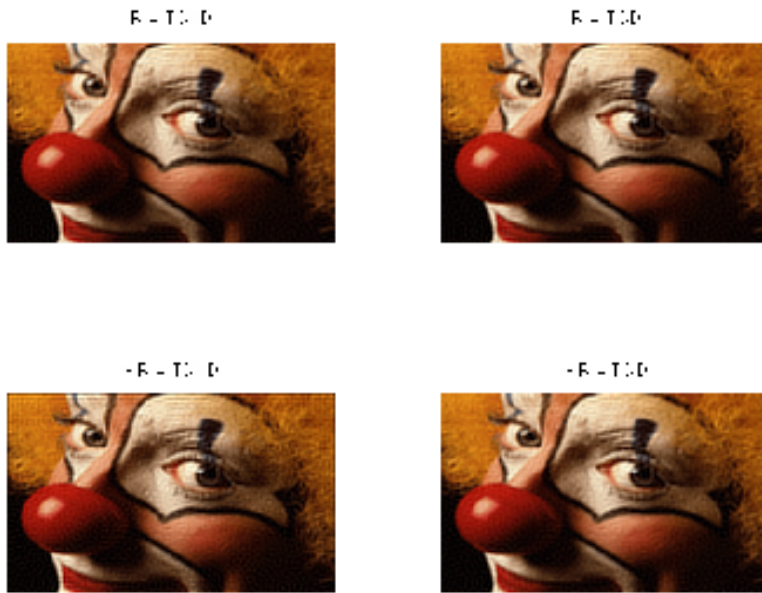
In Figure 5.4 is also reported the cross-channel blurred image with Gaussian PSF with support  $15 \times 15$  and  $\sigma_{i_1} = \sigma_{i_2} = 2$ . Notice that the entity of the cross-channel blurring is not negligible, since the whole image results to be darkened and the color intensities of the additive RGB system are substantially altered.

Table 5.4 reports the optimal RREs of truncated SVDs and SDs obtained by varying the dimension of the Gaussian PSF support and the parameter  $\rho$  related to the amount of the noise perturbation. It is worth stressing that we tune the filtering strategy with respect the spectral information given just by the matrix  $A_n$ , i.e., for any fixed  $\sigma_k$  (or  $\lambda_k$ ) we simultaneously sum, or discard, the three contribution on  $f$  related to the three singular values of  $A_{\text{color}}$ . In fact, the magnitude of singular values of the considered matrix  $A_{\text{color}}$  does not differ enough to dramatically change the filtering information given just by  $A_n$ . Nevertheless, also the comparison with the restoration results obtained by considering a global ordering justifies this approach. The color case behaves as the gray-scale one: as expected the optimal RRE becomes worse as the parameter  $\rho$  increases and the Anti-Reflective SD shows better performances in the case of low noise levels.

In addition, by referring to Figure 5.5, we note that the truncated SVD in the case of Anti-Reflective BCs shows a little more 'freckles' than the corresponding truncated SVD in the case of Reflective BCs. Nevertheless, for low noise levels, is just the Anti-Reflective SD that exhibits less 'freckles' than the Reflective SD.

**5.3. TIKHONOV AND RE-BLURRING REGULARIZATIONS.** By considering a Gaussian blurring of the true image reported in Figure 5.1, Table 5.5 compares the optimal RRE obtained in the case of the Tikhonov method for Reflective

$$\rho = 0.01$$



$$\rho = 0.05$$

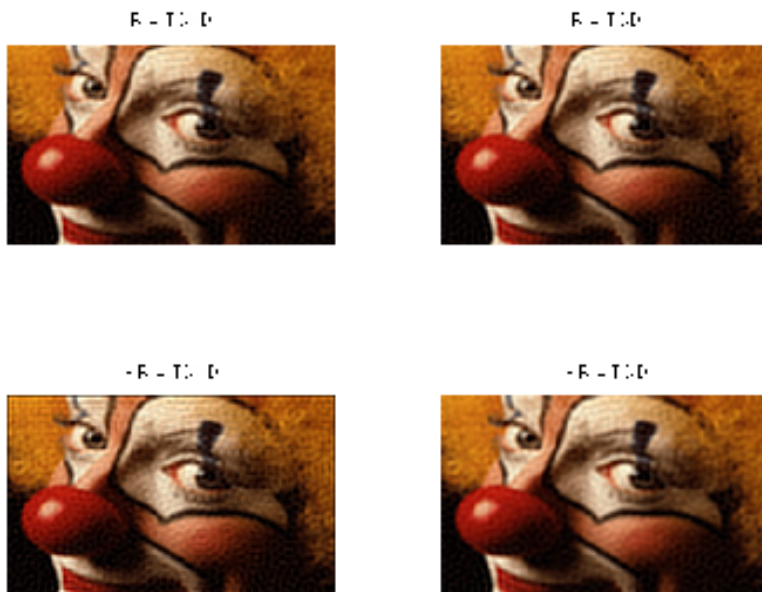


FIG. 5.5. Optimal restorations of truncated SVD and SD in the case of Reflective and Anti-Reflective BCs with reference to Figure 5.4 (Cross-channel and Gaussian Blur  $\sigma_{i_1} = \sigma_{i_2} = 2$ ).

TABLE 5.4

Optimal RREs of truncated SVD and SD with reference to the true image in Figure 5.4 (Cross-channel and Gaussian Blur  $\sigma_{i_1} = \sigma_{i_2} = 2$ ).

| Reflective BCs |          |         |         |         | Anti-Reflective BCs |          |          |         |         |
|----------------|----------|---------|---------|---------|---------------------|----------|----------|---------|---------|
| PSF            | 5x5      | 11x11   | 15x15   | 21x21   | PSF                 | 5x5      | 11x11    | 15x15   | 21x21   |
| $\rho = 0$     |          |         |         |         |                     |          |          |         |         |
| SVD            | 0.078276 | 0.12114 | 0.11654 | 0.1178  | SVD                 | 0.076646 | 0.1006   | 0.1098  | 0.10646 |
| SD             | 0.078276 | 0.12114 | 0.11654 | 0.1178  | SD                  | 0.074953 | 0.098474 | 0.10508 | 0.10216 |
| $\rho = 0.001$ |          |         |         |         |                     |          |          |         |         |
| SVD            | 0.078992 | 0.1212  | 0.11663 | 0.11792 | SVD                 | 0.077394 | 0.10639  | 0.1111  | 0.11002 |
| SD             | 0.078992 | 0.12119 | 0.11663 | 0.11792 | SD                  | 0.075727 | 0.10233  | 0.10612 | 0.10443 |
| $\rho = 0.01$  |          |         |         |         |                     |          |          |         |         |
| SVD            | 0.10152  | 0.12396 | 0.12088 | 0.12198 | SVD                 | 0.10431  | 0.12695  | 0.12624 | 0.12779 |
| SD             | 0.10152  | 0.12396 | 0.12088 | 0.12198 | SD                  | 0.10087  | 0.11737  | 0.11805 | 0.118   |
| $\rho = 0.05$  |          |         |         |         |                     |          |          |         |         |
| SVD            | 0.12102  | 0.13853 | 0.13743 | 0.13844 | SVD                 | 0.13017  | 0.15075  | 0.15063 | 0.15166 |
| SD             | 0.12102  | 0.13853 | 0.13743 | 0.13844 | SD                  | 0.12127  | 0.13699  | 0.13756 | 0.13795 |
| $\rho = 0.1$   |          |         |         |         |                     |          |          |         |         |
| SVD            | 0.13437  | 0.14898 | 0.14854 | 0.14947 | SVD                 | 0.1456   | 0.16516  | 0.16626 | 0.16647 |
| SD             | 0.13437  | 0.14898 | 0.14854 | 0.14947 | SD                  | 0.13507  | 0.14796  | 0.14955 | 0.15018 |

TABLE 5.5

Optimal RREs of Tikhonov and Re-blurring methods and corresponding  $\mu_{ott}$  with reference to the true image in Figure 5.1 (Gaussian Blur  $\sigma_{i_1} = \sigma_{i_2} = 2$ ).

| PSF            | 5x5      |          | 11x11    |          | 15x15    |          | 21x21    |          |
|----------------|----------|----------|----------|----------|----------|----------|----------|----------|
| $\rho = 0$     |          |          |          |          |          |          |          |          |
| R              | 0.041015 | 4.1e-005 | 0.079044 | 9e-006   | 0.086386 | 1.1e-005 | 0.089556 | 1.6e-005 |
| AR             | 0.034237 | 1.1e-005 | 0.059465 | 1e-006   | 0.078963 | 1e-006   | 0.079805 | 1e-006   |
| $\rho = 0.001$ |          |          |          |          |          |          |          |          |
| R              | 0.050155 | 0.000188 | 0.087482 | 5.7e-005 | 0.090825 | 4.3e-005 | 0.093071 | 4.9e-005 |
| AR             | 0.048556 | 0.000163 | 0.085279 | 4.6e-005 | 0.089388 | 3.3e-005 | 0.090821 | 3.3e-005 |
| $\rho = 0.01$  |          |          |          |          |          |          |          |          |
| R              | 0.083456 | 0.005555 | 0.10748  | 0.001786 | 0.10863  | 0.001678 | 0.11023  | 0.001573 |
| AR             | 0.083436 | 0.005536 | 0.10744  | 0.001792 | 0.10868  | 0.001691 | 0.11019  | 0.001575 |
| $\rho = 0.05$  |          |          |          |          |          |          |          |          |
| R              | 0.12024  | 0.038152 | 0.12982  | 0.01929  | 0.13071  | 0.018417 | 0.13307  | 0.017892 |
| AR             | 0.12049  | 0.038379 | 0.13006  | 0.01957  | 0.13096  | 0.018669 | 0.1333   | 0.018105 |
| $\rho = 0.1$   |          |          |          |          |          |          |          |          |
| R              | 0.14767  | 0.06587  | 0.14721  | 0.039231 | 0.14822  | 0.038181 | 0.15097  | 0.037893 |
| AR             | 0.14813  | 0.066251 | 0.14766  | 0.039707 | 0.14866  | 0.038644 | 0.15144  | 0.038296 |

BCs and of the Re-blurring method for Anti-Reflective BCs. In addition, in Table 5.6, the same comparison refers to the case of the Out-of-Focus PSF.

As expected, the RRE deteriorates as the dimension of the noise level or the dimension of the PSF support increases. Notice also that the gap between the Reflective and Anti-Reflective BCs is reduced also for low noise levels. Further numerical tests can be found in [9, 2].

Lastly, we focus our attention on the case of the color image in Figure 5.4. The image restorations have been obtained by considering the transformation procedure outlined at the end of Section 4. Despite the RREs in Table 5.7 are bigger than in the gray-scale case, the perception of the image restoration quality is very satisfying and a little less 'freckles' than in the corresponding SDs and SVDs are observed (see Figure 5.6). Notice, also that the lack of orthogonality in the  $S_{3n}$  transform related to the Anti-reflective BCs does not deteriorate the performances of the restoration.

**6. CONCLUSIONS.** In this paper we have analyzed and compared SD and SVD filtering methods in the case both of Reflective and Anti-Reflective BCs. Numerical evidence is given of the good performances achievable through SDs and with a substantially lower computational cost with respect to SVDs. In addition, the tensorial structure of the Reflective and Anti-Reflective SDs can be exploited in depth also in the case of not separable PSFs.

A special mention has to be done to the fact that the loss of orthogonality of the Anti-Reflective transform does not seem to have any consequence on the trend of the image restoration results. The analysis in the case of cross-channel blurring in color images allows to confirm the quoted considerations. Finally, the Re-blurring

TABLE 5.6

Optimal RREs of Tikhonov and Re-blurring methods and corresponding  $\mu_{ott}$  with reference to the true image in Figure 5.1 (Out-of-Focus blur).

| PSF | 5x5            |          | 11x11    |          | 15x15    |          | 21x21    |          |
|-----|----------------|----------|----------|----------|----------|----------|----------|----------|
|     | $\rho = 0$     |          |          |          |          |          |          |          |
| R   | 0.031422       | 0.000172 | 0.05346  | 6.9e-005 | 0.060954 | 3.5e-005 | 0.074785 | 2.7e-005 |
| AR  | 0.036213       | 0.000302 | 0.051236 | 6.8e-005 | 0.06683  | 5.7e-005 | 0.084482 | 5.8e-005 |
|     | $\rho = 0.001$ |          |          |          |          |          |          |          |
| R   | 0.034441       | 0.000271 | 0.061465 | 0.000145 | 0.073751 | 0.000101 | 0.09074  | 7.9e-005 |
| AR  | 0.038313       | 0.000402 | 0.059957 | 0.000138 | 0.076695 | 0.000126 | 0.095274 | 0.000106 |
|     | $\rho = 0.01$  |          |          |          |          |          |          |          |
| R   | 0.069647       | 0.008493 | 0.11361  | 0.004117 | 0.12881  | 0.003037 | 0.14914  | 0.001873 |
| AR  | 0.070384       | 0.008923 | 0.11404  | 0.00422  | 0.12982  | 0.003139 | 0.15061  | 0.001969 |
|     | $\rho = 0.05$  |          |          |          |          |          |          |          |
| R   | 0.12204        | 0.053687 | 0.1532   | 0.030719 | 0.16614  | 0.022121 | 0.18769  | 0.01346  |
| AR  | 0.12256        | 0.05423  | 0.15402  | 0.031574 | 0.16739  | 0.023213 | 0.18933  | 0.014472 |
|     | $\rho = 0.1$   |          |          |          |          |          |          |          |
| R   | 0.16366        | 0.092379 | 0.17357  | 0.055919 | 0.1829   | 0.042944 | 0.20323  | 0.028803 |
| AR  | 0.16433        | 0.093069 | 0.17485  | 0.057326 | 0.18457  | 0.044901 | 0.20511  | 0.031011 |

TABLE 5.7

Optimal RREs of Tikhonov and Re-blurring methods and corresponding  $\mu_{ott}$  with reference to the true image in Figure 5.4 (Cross-channel and Gaussian Blur  $\sigma_{i_1} = \sigma_{i_2} = 2$ ).

| PSF | 5x5            |          | 11x11    |          | 15x15   |          | 21x21    |          |
|-----|----------------|----------|----------|----------|---------|----------|----------|----------|
|     | $\rho = 0$     |          |          |          |         |          |          |          |
| R   | 0.069148       | 0.000203 | 0.11508  | 0.001204 | 0.1123  | 0.000717 | 0.11335  | 0.000726 |
| AR  | 0.062854       | 0.000102 | 0.091232 | 7e-006   | 0.1014  | 4.4e-005 | 0.098266 | 1.5e-005 |
|     | $\rho = 0.001$ |          |          |          |         |          |          |          |
| R   | 0.071259       | 0.000312 | 0.11515  | 0.001228 | 0.11239 | 0.000744 | 0.11347  | 0.000755 |
| AR  | 0.066734       | 0.000209 | 0.098658 | 5.8e-005 | 0.10276 | 7.7e-005 | 0.10111  | 4.5e-005 |
|     | $\rho = 0.01$  |          |          |          |         |          |          |          |
| R   | 0.094871       | 0.004975 | 0.11896  | 0.002919 | 0.11712 | 0.002421 | 0.1182   | 0.002459 |
| AR  | 0.094458       | 0.004841 | 0.1144   | 0.001884 | 0.11481 | 0.00184  | 0.11507  | 0.001755 |
|     | $\rho = 0.05$  |          |          |          |         |          |          |          |
| R   | 0.13209        | 0.029798 | 0.13662  | 0.015305 | 0.13599 | 0.014896 | 0.13669  | 0.014824 |
| AR  | 0.13239        | 0.029944 | 0.13561  | 0.014992 | 0.13593 | 0.014772 | 0.13611  | 0.014595 |

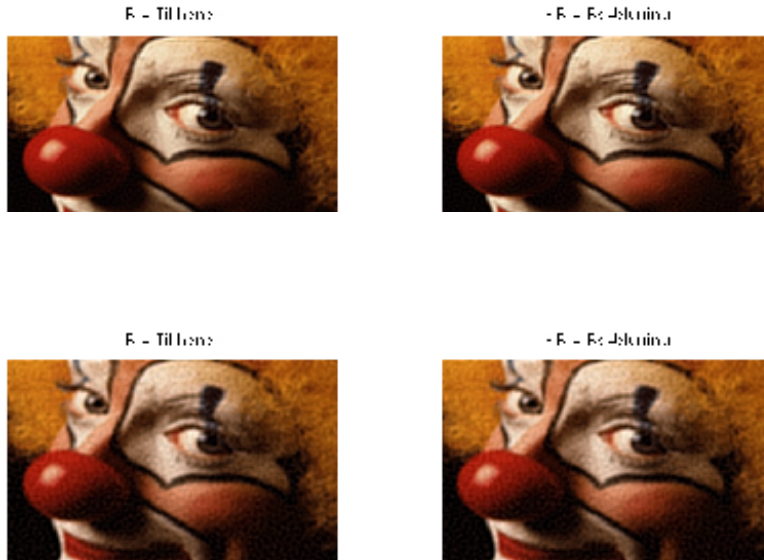


FIG. 5.6. Optimal RREs of Tikhonov and Re-blurring methods with reference to the true image in Figure 5.4 (Cross-channel and Gaussian blur  $\sigma_{i_1} = \sigma_{i_2} = 2 - \rho = 0.05$ ).

regularizing method has been re-interpreted as a standard Tikhonov regularization method in the space transformed by means of  $\tilde{T}_n$ . Some numerical tests highlight the image restoration performances, also in the case of cross-channel blurring.

Future works will concern the analysis of effective strategies allowing to properly choose the optimal regularizing parameters in the Anti-Reflective BCs case.

## REFERENCES

- [1] B. ANCONELLI, M. BERTERO, P. BOCCACCI, M. CARBILLET, AND H. LANTERI, *Reduction of boundary effects in multiple image deconvolution with an application to LBT LINC-NIRVANA*, *Astron. Astrophys.*, 448 (2006), pp. 1217–1224.
- [2] A. ARICÒ, M. DONATELLI, AND S. SERRA-CAPIZZANO, *The Antireflective Algebra: Structural and Computational Analyses with Application to Image Deblurring and Denoising*, *Calcolo*, to appear.
- [3] A. ARICÒ, M. DONATELLI, AND S. SERRA CAPIZZANO, *Spectral analysis of the anti-reflective algebra*, *Linear Algebra Appl.*, to appear.
- [4] A. ARICÒ, M. DONATELLI, J. NAGY, AND S. SERRA-CAPIZZANO, *The anti-reflective transform and regularization by filtering*, submitted, 2006.
- [5] M. BERTERO AND P. BOCCACCI, *Introduction to inverse problems in imaging*, Inst. of Physics Publ. London, UK, 1998.
- [6] M. BERTERO AND P. BOCCACCI, *Image restoration for Large Binocular Telescope (LBT)*, *Astron. Astrophys. Suppl. Ser.*, 147 (2000), pp. 323–332.
- [7] D. BINI AND M. CAPOVANI, *Spectral and computational properties of band symmetric Toeplitz matrices*, *Linear Algebra Appl.*, 52/53 (1983), pp. 99–125.
- [8] P. J. DAVIS, *Circulant Matrices*, Wiley, New York, 1979.
- [9] M. DONATELLI, C. ESTATICO, A. MARTINELLI, AND S. SERRA CAPIZZANO, *Improved image deblurring with anti-reflective boundary conditions and re-blurring*, *Inverse Problems*, 22 (2006), pp. 2035–2053.
- [10] M. DONATELLI, C. ESTATICO, J. NAGY, L. PERRONE, AND S. SERRA CAPIZZANO, *Anti-reflective boundary conditions and fast 2D deblurring models*, *Proceeding to SPIE's 48th Annual Meeting, San Diego, CA USA, F. Luk Ed, 5205* (2003), pp. 380–389.
- [11] M. DONATELLI AND S. SERRA CAPIZZANO, *Anti-reflective boundary conditions and re-blurring*, *Inverse Problems*, 21 (2005), pp. 169–182.
- [12] H. ENGL, M. HANKE, AND A. NEUBAUER, *Regularization of Inverse Problems*, Kluwer Academic Publishers, Dordrecht, The Netherlands, 2000.
- [13] C. W. GROETSCH, *The Theory of Tikhonov Regularization for Fredholm Integral Equations of the First Kind*, Pitman, Boston, 1984.
- [14] P. C. HANSEN, *Rank-deficient and discrete ill-posed problems*, SIAM, Philadelphia, PA, 1997.
- [15] M. HANKE AND J. NAGY, *Restoration of atmospherically blurred images by symmetric indefinite conjugate gradient technique*, *Inverse Problems*, 12 (1996), pp. 157–173.
- [16] P. C. HANSEN, J. NAGY, AND D. P. O'LEARY, *Deblurring Images Matrices, Spectra and Filtering*, SIAM Publications, Philadelphia, 2006.
- [17] R. L. LAGENDIJK AND J. BIEMOND, *Iterative Identification and Restoration of Images*, Springer-Verlag New York, Inc., 1991.
- [18] M. K. NG, R. H. CHAN, AND W. C. TANG, *A fast algorithm for deblurring models with Neumann boundary conditions*, *SIAM J. Sci. Comput.*, 21 (1999), no. 3, pp. 851–866.
- [19] L. PERRONE, *Kronecker Product Approximations for Image Restoration with Anti-Reflective Boundary Conditions*, *Numer. Linear Algebra Appl.*, 13–1 (2006), pp. 1–22.
- [20] F. ROSSI, *Tecniche di filtraggio nella ricostruzione di immagini con condizioni al contorno antiriflettenti*, (in Italian), Basic Degree Thesis, University of Milano-Bicocca, Milano, 2006.
- [21] S. SERRA CAPIZZANO, *A note on anti-reflective boundary conditions and fast deblurring models*, *SIAM J. Sci. Comput.*, 25–3 (2003), pp. 1307–1325.
- [22] Y. SHI AND Q. CHANG, *Acceleration methods for image restoration problem with different boundary conditions*, *Appl. Numer. Math.*, in press.
- [23] G. STRANG, *The Discrete Cosine Transform*, *SIAM Review*, 41–1 (1999), pp. 135–147.
- [24] C. R. VOGEL, *Computational Methods for Inverse Problems*, SIAM, Philadelphia, PA, 2002.